Soft Matter

RSC Publishing

PAPER

View Article Online
View Journal | View Issue

Effective pair potentials between nanoparticles induced by single monomers and polymer chains

Cite this: *Soft Matter*, 2013, **9**, 5916

Xue-Zheng Cao,[ab] Holger Merlitz,*[ab] Chen-Xu Wu,[a] S. A. Egorov[c] and Jens-Uwe Sommer[bd]

Using molecular dynamics (MD) simulations and density functional theory (DFT) calculations, we systematically study the effective pair potential between two particles induced by unconnected monomers and by polymers at various polymer concentrations (above the overlap), particle sizes, and polymer–particle interactions. In the case of athermal interactions, we verify that the entropic depletion forces between two nanoparticles inside a solvent of unconnected monomers oscillate in accordance with the radial distribution of monomers around one nanoparticle, and that the strength of polymer-induced entropic depletion forces rises linearly with the increase of nanoparticle size. These results are quite consistent with previously obtained experimental and theoretical results. When introducing attractive interactions between nanoparticles and polymers, the adsorption of polymer segments on the surface of each nanoparticle induces repulsive forces between the nanoparticles which can eliminate the depletion attractions. Enhancing the attraction between monomers and nanoparticles leads to the formation of thin polymer-layers on the surfaces of nanoparticles. As a consequence, the depletion attraction reappears at a somewhat increased particle distance. The observed phenomena become increasingly pronounced at higher polymer concentrations. Throughout this work we systematically compare computer simulation results with predictions from density functional theory and show that the data obtained with both approaches are quite consistent with each other.

Received 18th February 2013
Accepted 23rd April 2013

DOI: 10.1039/c3sm50495f

www.rsc.org/softmatter

I Introduction

The complex behavior of nanoparticle–polymer composites is of general interest not only within the polymer science community, but also in research areas like nanotechnology and biophysics. The mixing of polymers and nanoparticles is opening pathways for the engineering of flexible composites that exhibit advantageous electrical, optical, and mechanical properties.[1] While the understanding of materials at the micrometer and submicrometer scale has made significant progress in the past decades,[2] the current research on nanometer scales is still facing great challenges, since the phase behavior of polymer–nanoparticle composites is governed by an intricate balance of entropic and enthalpic forces. The combined effects of these forces, which occur at molecular scales, on their properties at mesoscopic and macroscopic scales is an active area of research with many unknowns.[3] Recent studies suggested several routes to exploit both enthalpic and entropic interactions in order to manipulate the phase behavior and thereby control the macroscopic performance of polymer–nanoparticle composites.[3–12] However, a separation of the different contributions to these interactions in experiment is difficult due to their delicate nature, and therefore our understanding of these nanoscopic phenomena in polymer–nanoparticle blends is yet incomplete.

The effective forces, being responsible for spontaneous structure formation, phase separation, or flocculation in polymer–nanoparticle composites, are in high demand to be understood in detail both from experimental and theoretical points of view. A first approximate explanation of the depletion forces was given by Asakura and Oosawa (AO),[13,14] who assumed that the dilute small spheres behave like an ideal gas, and that around each large sphere (or plate) a depletion zone exists which the centers of the small spheres cannot enter. Later A. Vrij introduced the AO model for particles immersed in polymers by approximating the ideal polymers as penetrable hard spheres with a size of the radius of gyration of the polymers.[15] The well-studied AO theory adequately describes the phase behaviors of polymer–colloid mixtures at dilute polymer concentrations in those situations in which polymer–polymer interactions are negligible and the particles are much larger than the coil size of polymers.[16–23] However, the modeling of the polymer coils as hard spheres turned out to be inaccurate for

[a]*Department of Physics and ITPA, Xiamen University, Xiamen 361005, P.R. China. E-mail: merlitz@gmx.de; cxwu@xmu.edu.cn*

[b]*Leibniz-Institut für Polymerforschung Dresden, 01069 Dresden, Germany*

[c]*Department of Chemistry, University of Virginia, Charlottesville, VA 22901, USA. E-mail: sae6z@virginia.edu*

[d]*Technische Universität Dresden, Institute of Theoretical Physics, D-01069 Dresden, Germany*

composites in the protein limit, in which the coil size of the polymers is larger than the nanoparticle size.[18,22,24–26] Further complications arise from the excluded-volume interactions between interacting polymers while increasing the concentrations, leading to phase diagrams that differ qualitatively from predictions of the classical AO theories.[10,27–31] In these cases, nanoparticles diffuse through a mesh of polymers, and the relevant length scale for the depletion forces becomes the polymer mesh size. Above the overlap density, the polymers are characterized by their correlation length, ξ, rather than their coil size R_g, so that the depletion forces exhibit a range proportional to ξ, which also defines the thickness of the polymer-depleted cavity.[32,33]

In a previous work, we had verified a scaling picture to understand the entropic depletion potentials between two nanoparticles induced by semi-dilute and concentrated polymers, while approximating the polymer matrix as a melt of correlation blobs.[34] According to this picture, the attraction between nanoparticles at a short distance is caused by the depletion of correlation blobs. In the present work, we analyze in detail the spatial distribution of polymer segments around two close nanoparticles and how the corresponding effective potentials between the nanoparticles are related to these distributions under various conditions. The general scaling predictions of the entropic depletion forces on the nanoparticle size and polymer concentration are verified, the results being quite consistent with previous theoretical predictions, including those from the microscopic polymer reference interaction site model (PRISM) and from density functional theory (DFT).[35–44]

Since the entropic depletion potential exhibits, at high polymer concentrations, a strong attraction at contact, it does not always support a stable homogeneous mixture of nanoparticles inside the polymer matrix. By using their PRISM model, Hooper and Schweizer predicted the existence of an enthalpically stabilized miscible state for polymer–nanoparticle composites if there existed a weak monomer–nanoparticle attraction.[7] Hence, a carefully designed attractive interaction between polymers and nanoparticles seemed to facilitate an improved miscibility. For strongly adsorbing polymers, a phase separation between polymers and polymer-covered nanoparticles was observed in both experiment[45] and theory.[7] Inspired by these results, we systematically investigate how the effective forces change with the increase of attraction and polymer concentration, thereby clarifying the physical mechanisms by which the organization of nanoparticles changes from contact aggregation to steric dispersion, and further to steric aggregation. Throughout this work, we combine results gained from MD simulations, which provide accurate data about both the forces between the nano-particles as well as density profiles and correlation functions, with DFT calculations which reduce the numerical effort and deliver fast results in symmetric situations. Otherwise, a bead–spring model and an equation of state which quantitatively corresponds to the MD simulation model were implemented.

Our work is structured as follows. In Section II, the simulation model and procedure to calculate the depletion forces are introduced in detail, and a brief introduction to the DFT is given. In Section III, we present and discuss the effective pair potentials between nanoparticles induced by unconnected monomers, athermal polymers, and attractive polymers. Our conclusions are given in Section IV.

II MD simulations and DFT

A Simulation model

The polymers are modeled using a coarse-grained bead–spring model without explicit twisting or bending potential, *i.e.* the bonds are freely rotating and freely jointed within the limits set by excluded volume interactions with nearby monomers. The beads represent spherical monomers which interact *via* a shifted Lennard-Jones (LJ) potential

$$U_{\mathrm{LJ}}(r) = 4\varepsilon\left[\left(\frac{\sigma_{\mathrm{M}}}{r}\right)^{12} - \left(\frac{\sigma_{\mathrm{M}}}{r}\right)^{6} - \left(\frac{\sigma_{\mathrm{M}}}{r_{\mathrm{c}}}\right)^{12} + \left(\frac{\sigma_{\mathrm{M}}}{r_{\mathrm{c}}}\right)^{6}\right], \quad (1)$$

where σ_{M} stands for the bead diameter and ε defines the strength of the interaction. The parameter r_{c} is the cut-off distance. It is easily verified that without any cutoff this potential has a minimum at $r_{\min} = 2^{1/6}\sigma_{\mathrm{M}}$ with the depth $U_{\mathrm{LJ}}(r_{\min}) = -\varepsilon$. In turn, once a cutoff $r_{\mathrm{c}} = 2^{1/6}\sigma_{\mathrm{M}}$ is implemented, the attractive contribution to this potential is eliminated and in this way athermal monomer–monomer interactions are simulated, being exclusively the case for all situations treated in this work.

The connectivity between monomers is enforced by a finite extensible nonlinear elastic (FENE) potential,[46] defined as

$$U_{\mathrm{FENE}}(r) = -0.5KR_0^2\ln\left[1 - \left(\frac{r}{R_0}\right)^2\right] + 4\varepsilon\left[\left(\frac{\sigma_{\mathrm{M}}}{r}\right)^{12} - \left(\frac{\sigma_{\mathrm{M}}}{r}\right)^{6}\right] + \varepsilon, \quad (2)$$

where the first term is attractive and extends to a maximum bond length of $R_0 = 1.5\sigma_{\mathrm{M}}$, whereas the second term, a LJ potential, contributes a short-range repulsion, which is cut off at $2^{1/6}\sigma_{\mathrm{M}}$, the minimum of the LJ-potential. The coefficient K is defined as $K = 30\varepsilon/\sigma_{\mathrm{M}}^2$, well tested in earlier studies;[47] this parameter set leads to an average bond length of $l_{\mathrm{av}} = 0.97\sigma_{\mathrm{M}}$.

The coarse graining of flexible polymers from the level of chemical monomers to the bead–spring model is based on sound principles of statistical mechanics.[48] The 'Kuhn-'monomers are of length scales at which orientation-correlations of bond-vectors, being a result of local bending potentials, cease, so that the polymer can be approximated as a freely jointed bead–spring chain. In this way, single monomers typically correspond to length scales of the order of nanometers.

In an athermal solvent, the interactions between nanoparticles with diameter σ_{NP} and monomers are modeled using a cut-off LJ-potential

$$U_{\mathrm{LJ}}(r) = 4\varepsilon\left[\left(\frac{\sigma_{\mathrm{MN}}}{r}\right)^{12} - \left(\frac{\sigma_{\mathrm{MN}}}{r}\right)^{6} - \left(\frac{\sigma_{\mathrm{MN}}}{r_{\mathrm{c}}}\right)^{12} + \left(\frac{\sigma_{\mathrm{MN}}}{r_{\mathrm{c}}}\right)^{6}\right], \quad (3)$$

where $\sigma_{\mathrm{MN}} = (\sigma_{\mathrm{NP}} + \sigma_{\mathrm{M}})/2$ is the mean size of the nanoparticle and monomer involved in the pair interaction, and the cut-off parameter r_{c} is chosen to cut the potential at its minimum, $r_{\mathrm{c}} = r_{\min} = 2^{1/6}\sigma_{\mathrm{MN}}$. In a subset of the simulations, the nanoparticle–monomer interactions are attractive. Here it is advisable, in

particular for nanoparticles of larger dimensions, to apply a short-range surface potential rather than the ordinary LJ-potential which would scale with the particle size. Hence we have implemented

$$U_{\mathrm{LJ}}(r) = 4\varepsilon\left[\left(\frac{\sigma_{\mathrm{M}}}{r-\Delta r}\right)^{12} - \left(\frac{\sigma_{\mathrm{M}}}{r-\Delta r}\right)^{6}\right], \quad (4)$$

with $\Delta r = \sigma_{\mathrm{MN}} - \sigma_{\mathrm{M}}$. A variation of the parameter ε then modifies the strength of the interaction. In all cases, the monomer–monomer interactions remained strictly repulsive (athermal). Note that pair interactions between the two nanoparticles were not required since we are interested in the effective forces imposed by the surrounding polymer matrix only.

The simulations were carried out using the open source LAMMPS molecular dynamics package.[49] In this work, the LJ system of units is used. It is defined using a model polymer with a LJ pair potential, featuring a bead size $\sigma_{\mathrm{M}} = 1$ (one length unit), a potential depth $\varepsilon = 1$ (one energy unit) and a mass $m = 1$ (one mass unit). The temperature is then normalized to that energy unit using a Boltzmann constant $K_{\mathrm{B}} = 1$, and the time unit is $\tau_{\mathrm{LJ}} = \mathrm{d}(m/\varepsilon)^{1/2}$, which is the oscillation time of a monomer inside the LJ potential, at small amplitudes so that the harmonic approximation is valid. The equation of motion for the displacement of a particle with index i is given by the Langevin equation:

$$m_i \frac{\mathrm{d}^2 \boldsymbol{r}_i}{\mathrm{d}t^2} = -\nabla U_i - \zeta \frac{\mathrm{d}\boldsymbol{r}_i}{\mathrm{d}t} + \boldsymbol{F}_i, \quad (5)$$

where $m_i = 1$ for monomers and $m_i = \left(\frac{\sigma_{\mathrm{NP}}}{\sigma_{\mathrm{M}}}\right)^3$ for nanoparticles, $\boldsymbol{r}_i$ is the position of the i^{th} particle, and U_i is the total conservative potential energy acting on the i^{th} particle. The quantity $\boldsymbol{F}_i$ is a random external force without drift and a second moment proportional to the temperature and the friction constant ζ. In our simulations, the temperature $T = 1$, a time-step $\Delta t = 0.001\tau_{\mathrm{LJ}}$, and the friction coefficient $\zeta = \tau_{\mathrm{LJ}}^{-1}$ were implemented.

B Simulation setup

In order to calculate effective forces between the two nanoparticles, we fixed one particle at the origin while the second one was attached *via* a stiff harmonic potential $f_{\mathrm{spring}}(r) = -k(r - r_0)$ with $k = 100$ as shown in Fig. 1, r_0 denotes the natural length of this spring potential. The harmonic potential is the only direct interaction between the two nanoparticles, enforcing a well defined average distance r over a large number of time-steps for each choice of r_0. The average distance r was then used to calculate the effective forces acting on the nanoparticles. More specifically, the equation

$$f_{\mathrm{spring}}(r) + f_{\mathrm{effective}}(r) + \frac{2}{r} = 0 \quad (6)$$

has to hold, where $f_{\mathrm{effective}}$ denotes the effective force induced by the surrounding polymer matrix. The additional term $2/r = \mathrm{d}[\ln \Omega(r)]/\mathrm{d}r$ is an entropic force related to the rotational degrees of freedom of the two-particle-system in three dimensions, in which $\Omega(r) \sim 4\pi r^2$. In eqn (6) we have expressed the force as a function of the average distance, instead of using ensemble-averaged forces. Since the fluctuations about r_0 remained very small, both approaches delivered identical results within the accuracy achieved in the simulations. Note that we set the energy unit to $k_{\mathrm{B}}T = 1$ in eqn (6) and in the following.

In order to calculate the depletion force as a function of particle-separation, $f_{\mathrm{effective}}(r)$, the value of r_0 was varied in separate simulations. Once the depletion forces were determined, the corresponding potential $U_{\mathrm{eff}}(r)$ was obtained through integration. The simulations were carried out in a periodic box of size $d = 24$, which is large enough to eliminate finite size effects. Throughout the paper, the volume ratio $c = N_{\mathrm{Monomer}}\pi{\sigma_{\mathrm{M}}}^3/6d^3$ was used to define the polymer concentration, where N_{Monomer} denotes the number of monomers inside the system. In our simulations, each system was relaxed by a simulation of 4×10^7 time-steps (corresponding to 4×10^4 LJ-times), followed by 10^8 time-steps (10^5 LJ-times) of data acquisition, during which a trajectory of 10 000 conformations was stored for the subsequent data analysis.

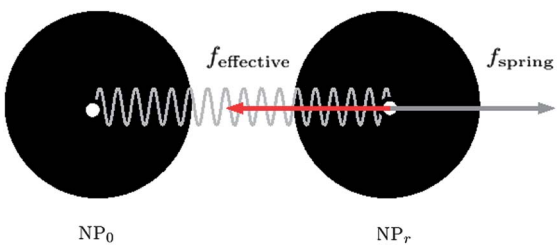

Fig. 1 Simulation setup to calculate the effective force between two nanoparticles. The nanoparticle NP_0 is fixed at the origin and connected with the second nanoparticle through a harmonic spring to enforce a well defined average distance.

C Density functional theory

In regard to DFT calculations, we note that all the details have been presented in our earlier publications,[39–44] and for the sake of brevity we only provide a brief summary here.

We consider two colloidal particles with diameter σ_{N} present at infinite dilution in a melt of fully flexible polymer chains composed of N tangent beads with a diameter σ_{M}. The intramolecular potential characterizing the polymer chain can be written as a sum of two terms:[39–44] the segment–segment excluded volume interaction potential V_{p} and the bonding energy V_{b}:

$$\begin{aligned} V(\boldsymbol{R}_{\mathrm{p}}) &= V_{\mathrm{p}}(\boldsymbol{R}_{\mathrm{p}}) + V_{\mathrm{b}}(\boldsymbol{R}_{\mathrm{p}}) \\ &= \sum_{i=3}^{N}\sum_{j=1}^{i-2} U_{\mathrm{LJ}}\left(|\boldsymbol{r}_i - \boldsymbol{r}_j|\right) + \sum_{i=1}^{N-1} v_{\mathrm{b}}(|\boldsymbol{r}_i - \boldsymbol{r}_{i+1}|), \end{aligned} \quad (7)$$

where $\boldsymbol{r}_i$ are the positions of the polymer beads ($\boldsymbol{R}_{\mathrm{p}} = \{\boldsymbol{r}_i\}$), and $v_{\mathrm{b}}(r)$ constrains adjacent beads to a fixed separation σ_{M}, *i.e.* $\exp[-\beta v_{\mathrm{b}}(r)] = \delta(r - \sigma_{\mathrm{M}})/4\pi{\sigma_{\mathrm{M}}}^2$, where $\beta = 1/k_{\mathrm{B}}T$. With the above form for $v_{\mathrm{b}}(r)$, one can write the total bonding energy as follows:

$$\exp\left[-V_{\mathrm{b}}(R_{\mathrm{p}})\right] = \prod_{i=1}^{N-1} \frac{\delta(|\boldsymbol{r}_i - \boldsymbol{r}_{i+1}| - \sigma_{\mathrm{M}})}{4\pi{\sigma_{\mathrm{M}}}^2}. \quad (8)$$

In order to obtain $U_{\mathrm{DEP}}(R)$, the polymer-mediated PMF between two colloids in a polymer solution, we define $\rho(\boldsymbol{r}, R)$ as the

conditional probability of finding a polymer bead at $\boldsymbol{r}$ given that one colloid is at the origin and the other one located at $\boldsymbol{R}$ ($R = |\boldsymbol{R}|$). With this definition, the polymer-mediated PMF between the two colloids is given by the following exact relations:[39–44]

$$U_{\mathrm{DEP}}(R) = \int_R^\infty f(R')\mathrm{d}R', \tag{9}$$

where the outwards excess mean force, $f(R)$, is given by:

$$\beta f(R) = \int \mathrm{d}\boldsymbol{r}(\nabla U_{\mathrm{LJ}}(r) \times \hat{\boldsymbol{R}})\rho(\boldsymbol{r},R). \tag{10}$$

It is clear from the above that $U_{\mathrm{DEP}}(R)$ is completely determined by the anisotropic bead density profile induced by the two colloids, $\rho(\boldsymbol{r})$ (to simplify the notation, from now on we suppress the explicit dependence of the density profile on the intercolloidal separation R). The average site density $\rho(\boldsymbol{r})$ is related to the density profile of the polymer melt, $\rho_{\mathrm{p}}(\boldsymbol{R}_{\mathrm{p}})$, as follows:

$$\rho(\boldsymbol{r}) = \int \mathrm{d}\boldsymbol{R}_{\mathrm{p}} \sum_{i=1}^{N} \delta(\boldsymbol{r} - \boldsymbol{r}_i)\rho_{\mathrm{p}}(\boldsymbol{R}_{\mathrm{p}}) \tag{11}$$

Hence, the problem of obtaining the polymer-mediated PMF reduces to the calculation of the equilibrium density profile of the polymer melt in an external potential created by a pair of colloidal particles, which we obtain from standard DFT formalism.

The starting point of the DFT treatment is the expression of the grand free energy, Ω, as a functional of the polymer density profile. The minimization of Ω with respect to $\rho_{\mathrm{p}}(\boldsymbol{R}_{\mathrm{p}})$ yields the equilibrium polymer density distribution. The functional Ω is related to the Helmholtz free energy functional, F, *via* a Legendre transform:

$$\Omega[\rho_{\mathrm{p}}(\boldsymbol{R}_{\mathrm{p}})] = F[\rho_{\mathrm{p}}(\boldsymbol{R}_{\mathrm{p}})] + \int \mathrm{d}\boldsymbol{R}_{\mathrm{p}}\rho_{\mathrm{p}}(\boldsymbol{R}_{\mathrm{p}})[V_{\mathrm{ext}}(\boldsymbol{R}_{\mathrm{p}}) - \mu], \tag{12}$$

where μ is the chemical potential and $V_{\mathrm{ext}}(\boldsymbol{R}_{\mathrm{p}})$ is the external field, which in the present case is due to the interaction of the polymer beads with the two colloids:

$$V_{\mathrm{ext}}(\boldsymbol{R}_{\mathrm{p}}) = \sum_{i=1}^{N} U_{\mathrm{LJ}}(\boldsymbol{r}_i) + \sum_{i=1}^{N} U_{\mathrm{LJ}}(|\boldsymbol{r}_i - \boldsymbol{R}|). \tag{13}$$

We employ the following approximation for the Helmholtz free energy functional, which separates it into ideal and excess parts according to:[39–44]

$$F[\rho_{\mathrm{p}}(\boldsymbol{R}_{\mathrm{p}})] = F_{\mathrm{id}}[\rho_{\mathrm{p}}(\boldsymbol{R}_{\mathrm{p}})] + F_{\mathrm{ex}}[\rho(\boldsymbol{r})], \tag{14}$$

with the ideal functional given by:[39–44]

$$\begin{aligned}\beta F_{\mathrm{id}}[\rho_{\mathrm{p}}(\boldsymbol{R}_p)] = {} & \int \mathrm{d}\boldsymbol{R}_{\mathrm{p}}\rho_{\mathrm{p}}(\boldsymbol{R}_{\mathrm{p}})[\ln \rho_{\mathrm{p}}(\boldsymbol{R}_{\mathrm{p}}) - 1] \\ & + \beta \int \mathrm{d}\boldsymbol{R}_{\mathrm{p}}\rho_{\mathrm{p}}(\boldsymbol{R}_{\mathrm{p}})V_{\mathrm{b}}(\boldsymbol{R}_{\mathrm{p}}).\end{aligned} \tag{15}$$

For the excess free energy functional we adopt the weighted density approximation:[39–44]

$$F_{\mathrm{ex}}[\rho(\boldsymbol{r})] = \int \mathrm{d}\boldsymbol{r}\rho(\boldsymbol{r})f_{\mathrm{ex}}(\bar{\rho}(\boldsymbol{r})), \tag{16}$$

with

$$\bar{\rho}(\boldsymbol{r}) = \int \mathrm{d}\boldsymbol{r}'\rho(\boldsymbol{r}')w(|\boldsymbol{r} - \boldsymbol{r}'|). \tag{17}$$

In the above, $f_{\mathrm{ex}}(\rho)$ is the excess free energy density per site of the polymer melt with site density ρ, $\bar{\rho}(\boldsymbol{r})$ is the weighted density, and $w(r)$ is the weighting function, which is normalized according to $\int \mathrm{d}\boldsymbol{r}w(r) = 1$.

The minimization of the grand free energy functional Ω yields the following result for the equilibrium polymer density profile:

$$\rho_{\mathrm{p}}(\boldsymbol{R}_{\mathrm{p}}) = \exp[-\beta(V_{\mathrm{ext}}(\boldsymbol{R}_{\mathrm{p}}) + V_{\mathrm{b}}(\boldsymbol{R}_{\mathrm{p}}) + \Lambda(\boldsymbol{R}_{\mathrm{p}}) - \mu)], \tag{18}$$

where

$$\Lambda(\boldsymbol{R}_{\mathrm{p}}) = \frac{\delta F_{\mathrm{ex}}}{\delta\rho_{\mathrm{p}}(\boldsymbol{R}_{\mathrm{p}})} = \sum_{i=1}^{N} \frac{\delta F_{\mathrm{ex}}}{\delta\rho(\boldsymbol{r}_i)}. \tag{19}$$

We now substitute the bonding energy from eqn (8), the external field from eqn (13), and the excess free energy from eqn (16) into eqn (18). The resulting polymer density profile $\rho_{\mathrm{p}}(\boldsymbol{R}_{\mathrm{p}})$ is then substituted into eqn (11) to obtain the following expression for the segment density profile:[39–44]

$$\rho(\boldsymbol{r}) = \frac{\rho_{\mathrm{b}}}{N} I[\rho(\boldsymbol{r})] \sum_{i=1}^{N} I_i[\rho(\boldsymbol{r})] I_{N+1-i}[\rho(\boldsymbol{r})], \tag{20}$$

where ρ_{b} is the segment bulk density. In the above expression:

$$I[\rho(\boldsymbol{r})] = \exp[-\beta(U_{\mathrm{LJ}}(\boldsymbol{r}) + U_{\mathrm{LJ}}(|\boldsymbol{r} - \boldsymbol{R}|) + \lambda(\boldsymbol{r}) - \lambda_{\mathrm{b}})], \tag{21}$$

and

$$I_i[\rho(\boldsymbol{r})] = \frac{1}{4\pi\sigma_{\mathrm{M}}^2} \int \mathrm{d}\boldsymbol{r}'\delta(|\boldsymbol{r} - \boldsymbol{r}'| - \sigma_{\mathrm{M}})I[\rho(\boldsymbol{r}')]I_{i-1}[\rho(\boldsymbol{r}')], \tag{22}$$

where $I_1[\rho(\boldsymbol{r})] \equiv 1$ and

$$\begin{aligned}\lambda(\boldsymbol{r}) &= f_{\mathrm{ex}}[\bar{\rho}(\boldsymbol{r})] + \int \mathrm{d}\boldsymbol{r}'\rho(\boldsymbol{r}')f_{\mathrm{ex}}'[\bar{\rho}(\boldsymbol{r}')]w(|\boldsymbol{r} - \boldsymbol{r}'|), \\ \lambda_{\mathrm{b}} &= f_{\mathrm{ex}}[\rho_{\mathrm{b}}] + \rho_{\mathrm{b}}f_{\mathrm{ex}}'[\rho_{\mathrm{b}}],\end{aligned} \tag{23}$$

with $f_{\mathrm{ex}}' = \mathrm{d}f_{\mathrm{ex}}/\mathrm{d}\rho$.

In order to compute $\rho(\boldsymbol{r})$ from eqn (20)–(23), it remains to specify the free energy per site $f_{\mathrm{ex}}(\rho)$ and the weighting function $w(r)$. For the free energy per site we adopt the result obtained on the basis of the first-order thermodynamic perturbation theory:[39–44]

$$f_{\mathrm{ex}}(\rho) = \frac{4\eta - 3\eta^2}{(1-\eta)^2} - \left(1 - \frac{1}{N}\right)\ln\frac{1 - \eta/2}{(1-\eta)^3} \tag{24}$$

where $\eta = \pi{\sigma_{\mathrm{M}}}^3\rho/6$ is the packing fraction. For the weighting function we employ the simple square-well form, whose range is given by the diameter of the polymer segment:

$$w(r) = \frac{3}{4\pi\sigma_{\mathrm{M}}^3}\Theta(\sigma_{\mathrm{M}} - r), \tag{25}$$

where $\Theta(r)$ is the Heaviside step function.

With the above definitions of $f_{\mathrm{ex}}(\rho)$ and $w(r)$, eqn (20)–(23) can be solved iteratively to obtain the site density profile $\rho(\boldsymbol{r})$. In

order to do this, we employ the direct inversion in iterative subspace algorithm.[39–44] Using the cylindrical symmetry of the problem, the anisotropic polymer site density around two colloidal particles is constructed on a two-dimensional grid: $\rho(\boldsymbol{r}) \equiv \rho(r, \theta)$. The convolutions in eqn (22) and (23) are performed by expanding the corresponding functions in Legendre polynomials.[39–44]

In performing numerical calculations, we found that using $N_l = 200$ Legendre polynomials was sufficient to obtain converged results for colloid–polymer systems discussed in the next Section. The step size along the radial coordinate of the grid was taken to be $0.05\sigma_M$, and the number of points along this coordinate ranged from 300 to 400 depending on the size of the colloidal particle. Once the polymer site density profile was calculated from eqn (20)–(23), it was substituted into eqn (10) to compute the excess mean force between the two colloids, from which the polymer-mediated PMF was obtained *via* eqn (9). The integral in eqn (9) was calculated on a grid with step size $0.05\sigma_M$.

III Results and discussion

In what follows we shall denote contributions to the nanoparticle pair potential in an athermal solvent, which are entirely of entropic origin, as $U_{DEP}(r)$, the entropic depletion potential. They will be discussed in detail in Section III A and III B. In the case of attractive potentials between polymers and nanoparticles there exists a subtle interplay between both entropic and enthalpic contributions, the corresponding effective pair potentials shall be denoted as $U_{EFF}(r)$ and studied in Section III C.

A Entropic depletion potential induced by disconnected monomers

We firstly discuss a setup of two nanoparticles inside a solution of single (disconnected) monomers, *i.e.* polymer chain length $N = 1$, which serves as a first step towards the understanding of polymer-induced entropic depletion potentials. The nanoparticle size is $\sigma_{NP} = 3\sigma_M$, at various monomer packing fractions in the range between $c = 0.0969$ and $c = 0.388$. At low monomer concentrations and volume fractions of $c < 0.10$, the potential exhibits a weak short-range attraction, which at higher density increases in strength and additionally begins to oscillate as shown in Fig. 2. The first of these oscillations generates a pronounced repulsive barrier surrounding the short-range attractive region. As shown in the figure, our DFT results are seen to be in good agreement with computer simulations, reproducing all the general trends observed. These oscillatory depletion potentials are in qualitative agreement with experimental results obtained with a line-scanned optical tweezer[50] for large sized colloid particles immersed in a sea of small particles, *i.e.* $\sigma_{NP} \gg \sigma_M$.

The oscillations, which are not contained in the AO model,[13,14,51] can be explained by the fact that at higher concentrations the monomers tend to form layers around the nanoparticles as a result of a surface-induced short-range ordering, similar to a liquid in the vicinity of a hard boundary. Whether or not the effect of the higher order layers is significant

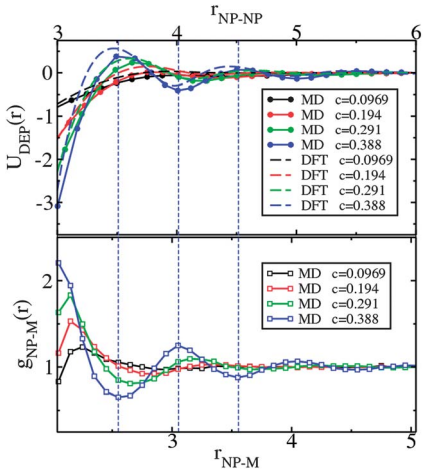

Fig. 2 MD simulation and DFT results for the entropic depletion potentials between two nanoparticles of size $\sigma_{NP} = 3\sigma_M$ as induced by a solution of (disconnected) monomers at different concentrations. The lower panel displays the corresponding radial distributions of monomers around a single nanoparticle. To show the correlation between the depletion potential and the radial distribution for one example at polymer concentration $c = 0.388$, dotted straight lines are plotted to guide the view.

does strongly depend on the total volume fraction of monomers. The oscillatory behavior of the depletion potentials is far more pronounced at higher monomer densities. The corresponding radial distributions of monomers around a single nanoparticle, $g_{NP-M}(r)$, are also plotted in the lower panel of Fig. 2, indicating the short-range ordering of hard-sphere monomers around the nanoparticle. There exists a significant accumulation of monomers near the surface of the nanoparticle, which results in the substantial peak of the first layer. Once the two nanoparticles approach one another, the densely packed layers of monomers around each nanoparticle begin to interact, generating the repulsive peaks in the corresponding depletion potential. In order to reach the primary short-range attractive region, the two nanoparticles must firstly squeeze out the dense monolayers in between, generating a void in between both particles, which leads to the strong density gradient that attracts the nanoparticles.

Taking a closer look at the plots of $g_{NP-M}(r)$ and $U_{DEP}(r)$ in Fig. 2, we observe a clear correlation: minima of the particle density correspond to maxima of the depletion potential and *vice versa*. In consistence with the experimental observation in ref. 50, we note that the oscillation wavelength of the depletion potential l, *i.e.* the periodic distance between two neighboring repulsive peaks, is comparable to the mean spacing between the matrix monomers (averaged mass-center distance between monomers) in the fluid state. Whenever the gap between the surfaces of the nanoparticles amounts to a multiple integer of l, the potential displays a minimum, and consequently there exists a maximum at separations of half-integer multiples of l.

In order to illustrate how the depletion potential arises from the monomer density distributions in the vicinity of the nanoparticle, we have computed two-dimensional cross-sections from the simulation data. Fig. 3 displays the densities at the monomer concentration of $c = 0.291$. The data were averaged

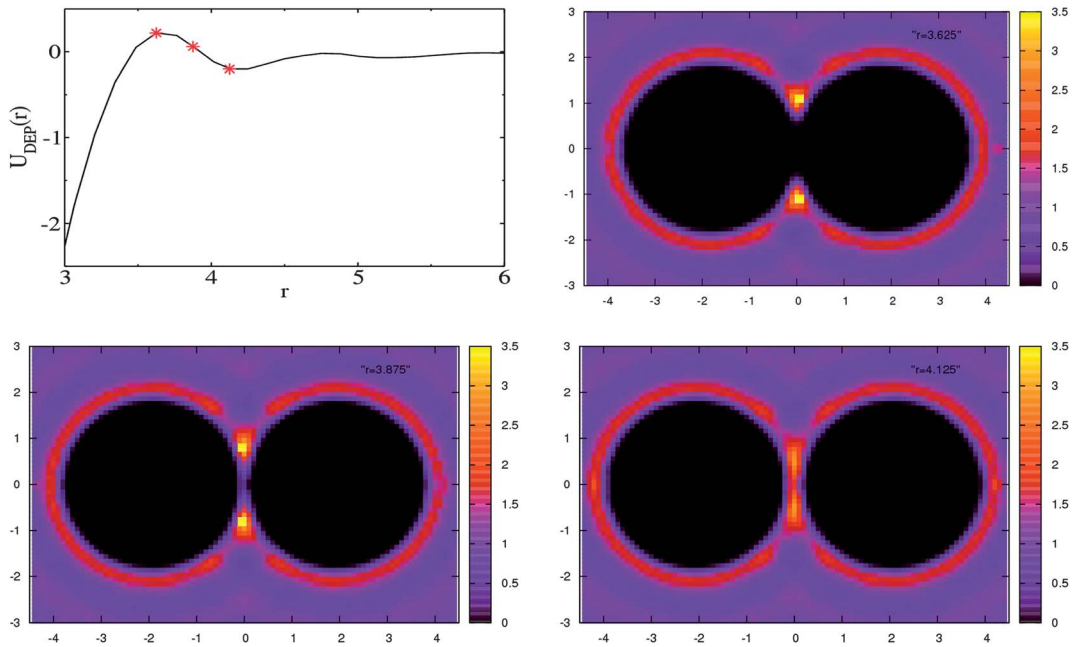

Fig. 3 Entropic depletion potential induced by unconnected monomers at $c = 0.291$ (upper left), and corresponding two dimensional density profiles of monomers around the nanoparticle setup at three different separations, the positions being marked in the plot of the effective potential. Here, $\sigma_{NP} = 3\sigma_M$.

over 6000 conformations or 6×10^7 time-steps. Clearly discernible are several concentric rings of high monomer density exterior to the nanoparticles, a result of the short-range packing of monomers. The most inner rings have the highest monomer densities, and at a nanoparticle separation of about $r = 4.125$, they begin to overlap and generate the observed repulsive force. Upon further approach of the nanoparticles, a void between them begins to form at $r = 3.875$, since now the monomers become sterically expelled from the overlap region. At a close distance ($r \leq 3.625$), an attraction arises due to the osmotic pressure difference between the external matrix and the empty depletion volume, leading to the attractive short-range potential. Note that even in this latter case, there exist certain regions at the boundary of the void with significantly increased monomer densities (as coded in yellow).

B Entropic depletion potential induced by athermal polymers

Once the nanoparticles are placed inside a matrix of athermal polymers at concentrations well above the overlap, the physical conditions become different.[52,53] The two-dimensional density profiles of monomers around the nanoparticles at a polymer concentration $c = 0.291$ are shown in Fig. 4. Short-range packing effects as they were observed with disconnected monomers are still visible, though less pronounced. Monomer densities do not reach as high values, even in the overlap region, as in the disconnected case, and therefore the repulsive forces triggered by polymers are comparably weak. The weakness of the repulsive forces may be one reason for the absence of any repulsive barrier in the polymer-induced depletion potential of former experimental[32] and theoretical results.[8,54] At a distance of $r = 4.125$ between the two nanoparticles, monomers are still depleted from the overlap zone, quite in contrast to the case of disconnected monomers in which they largely aggregated between the nanoparticles.

A quantitative comparison of the scaling model and simulations has been presented in a previous work by the authors,[34] supporting the validity of a picture, in which the polymer matrix is approximated as a melt of soft particles of the size of the correlation blob. Above the overlap concentration, $c > c^*$, the depletion potential is therefore independent of the chain length N or polydispersity of the polymers, displaying a universal behavior for $N \gg g$, where g is the average number of monomers inside one correlation blob. Based on that scaling theory, we derived a depletion force between the nanoparticles at the surface contact, scaling as $f_0 = f(r = \sigma_{NP}) \sim \sigma_{NP}\Pi^{2/3}$, where Π denotes the osmotic pressure. To test this prediction, the contact force as a function of the directly measured osmotic pressure was analyzed and a close agreement with the scaling law $f_0 \sim \Pi^{2/3}$ was obtained.[34] The linear dependence of f_0 on the nanoparticle size σ_{NP} is tested in the upper panel of Fig. 5, being valid over a wide range of polymer concentrations. In addition, far above the overlap concentration, *i.e.* $c \gg c^*$, the lower panel of Fig. 5 shows a scaling behavior of the contact force with the polymer concentration obtained by both MD and DFT. The approximate fitting of $f_0 \sim c^2$ implies that the osmotic pressure increases largely according to $\Pi \sim c^3$ within the crossover region investigated here.

It should be noted that the generic widening of the fluid–solid transition of a polymer–nanoparticle composite has been found to be primarily driven by the value of the depletion force at contact.[8,55] The universal scaling law of $f_0 \sim \sigma_{NP}\Pi^{2/3}$, which appears fairly robust within our simulations, promises to be a valuable step towards the understanding and optimization of these polymer–nanoparticle composites. Decreasing the

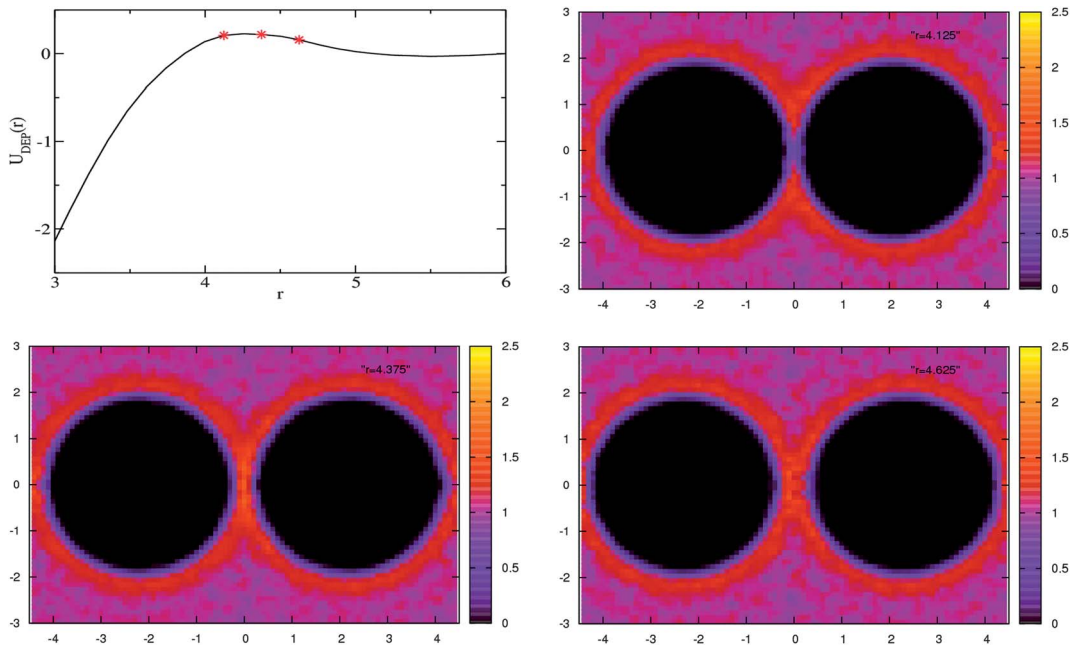

Fig. 4 Induced entropic depletion potential between nanoparticles inside a polymer matrix ($N = 64$) at polymer concentration $c = 0.291$ (upper left), and two-dimensional monomer density profiles. The polymer–nanoparticle interaction is athermal. Here, $\sigma_{NP} = 3\sigma_M$.

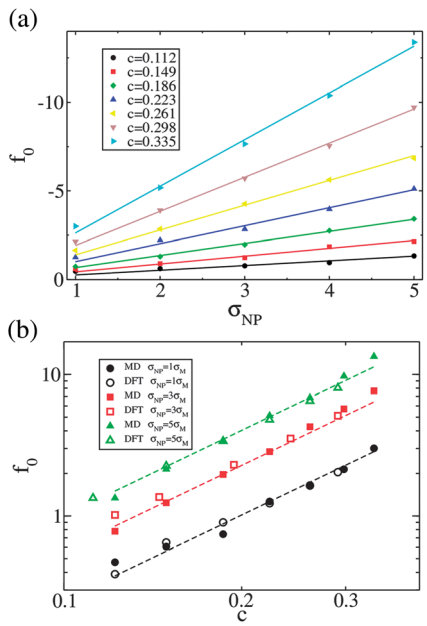

Fig. 5 Contact forces: (a) the upper panel displays a linear dependence of f_0 on the nanoparticle size σ_{NP} at different concentrations c, the straight lines being linear fits; (b) the lower panel shows the scaling dependence of f_0 on monomer concentration c for three different nanoparticle sizes, dotted straight lines having the same slopes $f_0 \sim c^2$. The polymer length was $N = 64$.

polymer concentration or reducing the nanoparticle size is expected to improve the dispersion of nanoparticles inside the polymer matrix, since in this way the interaction strength of the depletion potential is reduced.

At this point we have shown that the nanoparticle size σ_{NP} is playing a critical role in defining the magnitude of the depletion potential and hence the phase structure of polymer–nanoparticle composites, and how the contact forces are scaling with that particle size. In both scaling and PRISM model, the linear dependence of the depletion force on the nanoparticle size has been predicted to be valid not only at contact, but at any nanoparticle-separation.[33,37] In order to verify these predictions in the framework of our MD-simulations, we computed the polymer-induced entropic depletion potentials between two nanoparticles, for systems at a constant polymer concentration, $c = 0.291$, and increasing nanoparticle sizes $\sigma_{NP} = 2.0$, 3.0, 4.0 and 5.0. The data are horizontally shifted by the nanoparticle size, *i.e.* plotted as a function of the gap distance $x = r - \sigma_{NP}$, and scaled with the nanoparticle size, as displayed in Fig. 6. The attractive parts of the plots fall onto the same master curve. The repulsive parts display minor individual differences, which turn

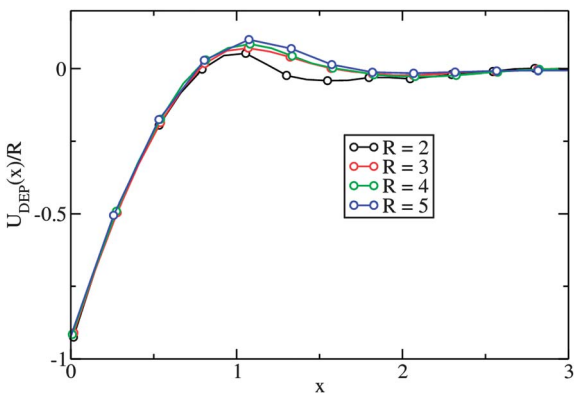

Fig. 6 Polymer induced entropic depletion potentials for different nanoparticle sizes σ_{NP} and fixed $c = 0.291$. R is the ratio σ_{NP}/σ_M, and $x = r - \sigma_{NP}$ the surface distance between the nanoparticles.

significant only in the case of the smallest particle, $\sigma_{NP} = 2.0$. Note that in this latter case, the correlation blob size ($\xi \approx 2.5$ at $c = 0.291$) already exceeds the nanoparticle size and the picture of blobs that have to be expelled from the gap between both particles is breaking down. We may therefore conclude that the linear dependence of the depletion forces on the nanoparticle size is verified, as long as the particle size exceeds the correlation length of the polymer matrix.

C Effective pair potential induced by attractive polymers

Since the entropic depletion potential generally exhibits a strong attraction at contact, it does not always support a stable homogeneous mixture of nanoparticles inside the polymer matrix. Previous studies indicate that nanoparticle–polymer mixtures did phase separate at high nanoparticle concentrations.[11,56–58] The possible aggregation of nanoparticles negates the advantageous properties of polymer–nanoparticle composites associated with their nanoscopic dimension. As part of the renewed interest in nanocomposites, researchers began seeking for methods to control the dispersion of nanoparticles in polymeric hosts.[1,4]

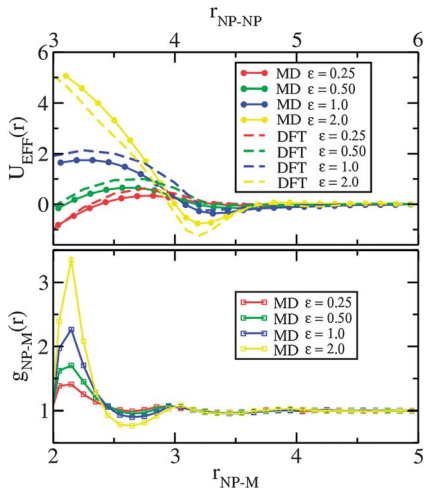

Fig. 7 MD and DFT results for the effective pair potentials between nanoparticles induced by attractive polymers for different values of the polymer–nanoparticle interaction parameter ε at polymer concentration $c = 0.291$ (upper panel), and the corresponding radial distribution of monomers around one nanoparticle (lower panel). Here, $N = 64$ and $\sigma_{NP} = 3\sigma_M$.

A thermodynamically stable dispersion of nanoparticles inside a polymer liquid may be achieved for systems with an attractive interaction between polymers and nanoparticles. In this way the entropically unfavorable mixing of both components, due to the entropically controlled depletion attraction, is facilitated by an enthalpy gain from polymer–nanoparticle contacts. Hence, attractive interactions between polymers and nanoparticles seem to be required to achieve an improved miscibility, and the dispersion of nanoparticles in their polymeric hosts. With their PRISM model, Hooper and Schweizer. have predicted the abrupt transition of polymer–nanoparticle composites from a state that is phase separated through the entropic depletion attraction, to another, enthalpically stabilized miscible phase, after adding an enthalpic attraction between nanoparticles and monomers.[7]

In Fig. 7, the effect of polymer–nanoparticle attraction on the effective pair interaction between the nanoparticles is investigated for different values of the interaction parameter ε (see eqn (4)). As expected, the dominant effect of adding a nanoparticle–polymer attraction is the elimination of the entropic short-range depletion attraction from the effective potential. This attraction is gradually replaced by a repulsion as the enthalpic attractions between the polymer and nanoparticle increase in strength. The corresponding radial distributions of polymer segments around one single nanoparticle are shown in the lower panel of Fig. 7, their densities being significantly enhanced near the surface contact. Upon approach of both nanoparticles, these monomers have to be squeezed out, against their enthalpic attraction, leading to the effective short-range repulsion of the nanoparticles. DFT results, which are also presented in Fig. 7 show the same effect of polymer–nanoparticle attraction on the effective pair interaction between the nanoparticles, and are in close agreement with the MD simulations. Two-dimensional density profiles for the case of $\varepsilon = 1.0$ at separations of $r = 3.5$ and $r = 4.0$ are shown in the snapshots of Fig. 8, the highlighted spots indicating high monomer densities and correspondingly strong repulsive forces upon overlap.

The effective pair interaction between the nanoparticles largely determines the stability of a suspension of nanoparticles mixed inside the polymer host, though, at higher concentrations, additional many-body effects have to be included for an elaborate understanding of the phase behaviors of

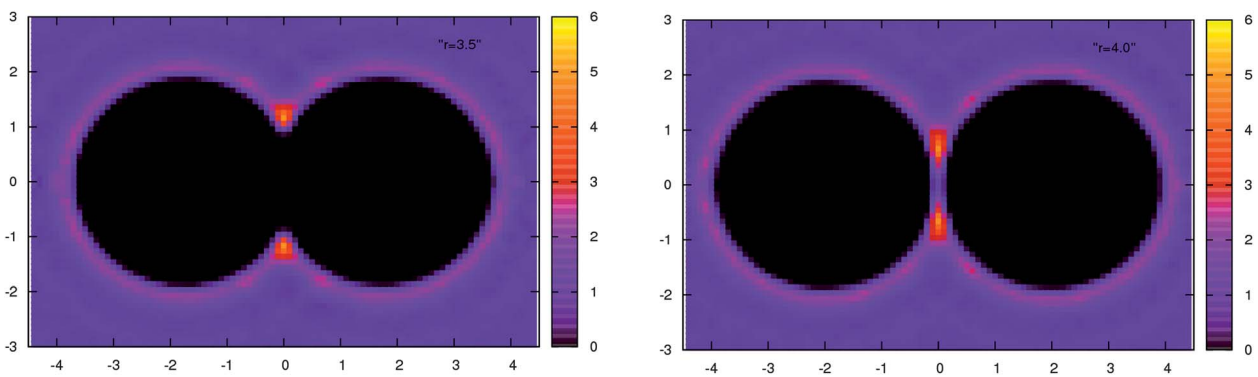

Fig. 8 Snapshots of two-dimensional density profiles of monomers around the nanoparticles at $r < r_m$, for the case of $c = 0.291$ and $\varepsilon = 1.0$. Here $N = 64$ and $\sigma_{NP} = 3\sigma_M$.

polymer–nanoparticle composites. A convenient measure of the effect of the pair interaction is the second osmotic virial coefficient B_2, which is sensitive to the strength and range of the effective interaction, and defined as

$$B_2 = B_2^{HS} + 2\pi \int_{\sigma_{NP}}^{\infty} r^2 \left(1 - e^{-U_{EFF}(r)}\right) dr, \quad (26)$$

where $B_2^{HS} = 2\pi\sigma_{NP}^3/3$ is the second virial coefficient of a system of hard spheres with diameter σ_{NP}. The normalized second virial coefficients $B_2^* = B_2/B_2^{HS}$ were measured and are shown in Fig. 9 as a function of the interaction strength, ε, and at a fixed polymer concentration $c = 0.291$. As a general tendency an increase of B_2^* with ε is observable. In particular B_2^* significantly increases during the addition of polymer–nanoparticle attraction, when compared to the athermal situation in which $B_2^*(c = 0.291) = -0.667$. This supports the conjecture that an enthalpic stabilization of the dispersion of nanoparticles is possible.

However, there exists a potential pitfall: following the repulsive part of $U_{EFF}(r)$, exterior to the potential minimum distance $r = r_{min}$, there exists an extended attraction zone which is weak but clearly visible especially at high interaction strengths. Note that the second virial coefficient approaches a constant value after the monomer–nanoparticle attraction strength is larger than about one *KT*. To clarify the origin of this extended attraction, it is instructive to take another look at the radial distributions of monomers around each nanoparticle (lower panel of Fig. 7). At high interaction strength, the monomers form a dense layer, generating polymer-dressed nanoparticles with increased effective size, a phenomenon that has also been reported in recent experiments.[45] Those dressed nanoparticles behave similar to the bare nanoparticles in an athermal polymer matrix, with a depletion cavity at close distances which resembles the properties of a LJ-type potential. Hence, if the attraction between nanoparticles and polymers is chosen too strong, the enthalpic stabilization of the mixture is outbalanced by the entropic depletion force between the polymer-dressed nanoparticles. It is therefore mandatory to choose the enthalpic interactions between both components with great care in order to achieve the desired stabilization.

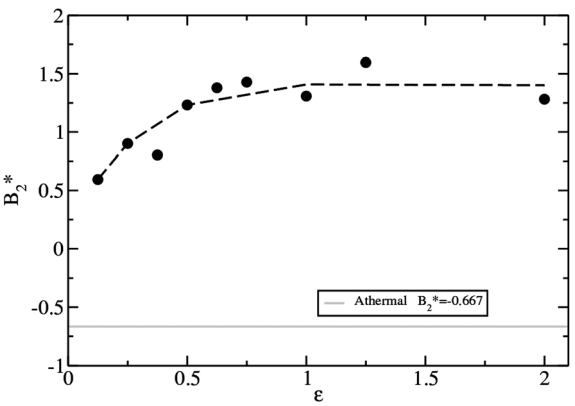

Fig. 9 The reduced second virial coefficient B_2^* as a function of the interaction strength ε; the dotted line is used to guide the eye. Here, $c = 0.291$, $N = 64$ and $\sigma_{NP} = 3\sigma_M$.

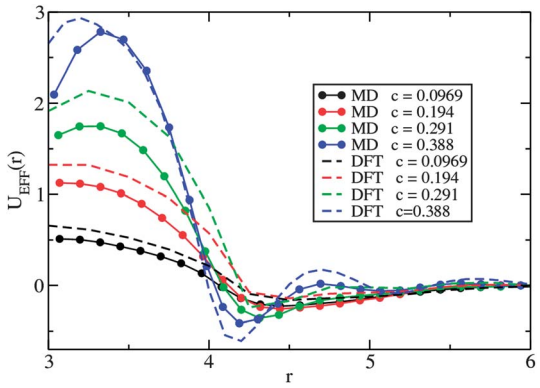

Fig. 10 MD and DFT results for the effective pair potentials between nanoparticles induced by attractive polymers for different c and fixed $\varepsilon = 1.0$. Here $N = 64$ and $\sigma_{NP} = 3\sigma_M$.

Finally, we investigate the influence of polymer concentration on the effective interaction potentials. These, obtained from MD simulations and from DFT calculations at fixed interaction strength $\varepsilon = 1.0$, are shown in Fig. 10. The two methods deliver mutually consistent results that display the same general trends, though deviating somewhat in their quantitative predictions, in particular at high polymer concentrations. Among the common trends are the repulsive part (due to the adhesion of monomers onto the nanoparticle surface) and the exterior depletion attractions that are intensified with the increase of the polymer concentration. At higher polymer concentrations, there are a larger number of monomers attached on the nanoparticle surface. The pair nanoparticles need to pay higher energy compensation to squeeze out the surrounding monomers, hence the effective repulsion is improved by increasing the polymer concentration. At the same time, the depletion force acting on the pair nanoparticles saturated with the monomer-layer is enhanced since more monomers in bulk contribute to the higher osmotic pressure after the polymer concentration is increased. So the total effect of increasing the polymer concentration, when the monomer–nanoparticle attraction is strong, is to improve the probability of a demixing phase separation between polymers and polymer-covered nanoparticles. Although the observed extended depletion attraction is not as strong as in the case of athermal polymers, a demixing phase separation between polymers and polymer-covered nanoparticles is expected to happen for polymer–nanoparticle blends at polymer concentrations exceeding those necessary to saturate the nanoparticle surface.[45] Note that the origin of this phase separation is not related to the reported flocculation of nanoparticles that are bridged by strongly adsorptive polymers at relatively low concentrations.[7,45]

IV Conclusion

In summary, the effective pair potentials between nanoparticles induced by unconnected monomers, by athermal polymers and

attractive polymers above the overlap concentration have been calculated directly using MD simulations and additionally computed *via* the density functional theory. The entropic depletion forces that arise between two nanoparticles inside a solvent of smaller monomers are verified to be oscillatory. A clear correlation is observed between the calculated entropic depletion potentials and the ordering of monomers packed around nanoparticles. Whenever the gap between the surfaces of the nanoparticles is commensurate with the monomer layers, the free energy displays a minimum, with a local maximum whenever they are incommensurate. This implies that the liquid structure of unconnected monomers induces the oscillatory entropic depletion potential between the two nanoparticles.

We have thoroughly verified the validity of the scaling model of the polymer-induced entropic depletion potential, through variation of the polymer concentration and the nanoparticle size. Apart from the scaling properties associated with the polymer matrix, the nanoparticle size plays a critical role in deciding the strength of the depletion force at contact, f_0, which is increasing linearly with the nanoparticle diameter. The universal scaling law, $f_0 \sim \sigma_{NP}\Pi^{2/3}$, was found to be very robust throughout the entire set of simulation data, and is likely to be of significant help for the development and understanding of polymer–nanoparticle composites. Our data further prove that the linearity between the depletion force and the particle size remains valid not only at contact, but for the entire interaction range of the depletion potential, as long as the nanoparticle size remains larger than the correlation length of the polymer matrix.

Enthalpic attractive interactions between nanoparticles and polymers induce repulsive forces between the nanoparticles which are shown to eliminate the depletion attractions. This could be a pathway to facilitate the dispersion of nanoparticles inside polymeric matrices. Strong adsorption, on the other hand, can lead to the formation of a thin polymer layer on the surfaces of nanoparticles. In this way, the now "dressed" nanoparticle is effectively an athermal particle of increased size which once again induces a depletion attraction beyond the repulsive core, which would lead to an undesired demixing of both components. The optimal setup for dispersing NPs in a dense polymer matrix is achieved after tuning the monomer–nanoparticle attraction to a value of the order *KT*, for instance through modification of the particle surface. Then the depletion attraction is almost cancelled, and a strong adsorption layer which favors depletion attraction of the "dressed" particles is not yet formed. The same argument holds for the brush-coating of NPs that is often applied to compatibilize the composites. Here the usually irreversibly adsorbed polymer brush induces a depletion attraction and soft-repulsion at overlap. Varying the grafting density, however, can lead to the same, compatibilizing effect as is observed with the weakly adsorbed polymers in our study.

It is further shown that both the repulsive and attractive parts of this effective potential increase with the polymer concentration. Care has to be taken with the choice of system parameters to facilitate an optimum dispersion of the nanoparticles inside the polymer matrix. Finally, throughout this work we have systematically compared computer simulation results with density functional theory predictions, both being quite consistent with each other, delivering the same qualitative trends with just moderate quantitative differences at high polymer concentrations.

Acknowledgements

This work was partly supported by the National Science Foundation of China under grant nos. 10974162 and 11074208.

References

1 A. C. Balazs, T. Emrick and T. P. Russell, *Science*, 2006, **314**, 1107.
2 M. Stamm and J.-U. Sommer, *Nat. Mater.*, 2007, **6**, 260.
3 E. S. McGarrity, A. L. Frischknecht and M. E. Mackay, *J. Chem. Phys.*, 2008, **08**(128), 154904.
4 M. E. Mackay, A. Tuteja, P. M. Duxbury, C. J. Hawker, B. V. Hom, Z. Guan, G. Chen and R. S. Krishnan, *Science*, 2006, **311**, 1740.
5 Z. Zhang and J. S. van Duijneveldt, *Langmuir*, 2006, **22**, 63.
6 A. M. Kulkarni, A. P. Chatterjee, K. S. Schweizer and C. F. Zukoski, *Phys. Rev. Lett.*, 1999, **83**(22), 4554.
7 J. B. Hooper and K. S. Schweizer, *Macromolecules*, 2006, **39**, 5133.
8 R. Tuinier and G. J. Fleer, *Macromolecules*, 2004, **37**, 8764.
9 R. Dickman and A. Yethiraj, *J. Chem. Phys.*, 1993, **100**(6), 4683.
10 P. G. Bolhuis, A. A. Louis and J.-P. Hansen, *Phys. Rev. Lett.*, 2002, **89**(12), 128302.
11 P. G. Bolhuis, E. J. Meijer and A. A. Louis, *Phys. Rev. Lett.*, 2003, **90**(6), 068304.
12 M. Fuchs and K. S. Schweizer, *Phys. Rev. E: Stat., Nonlinear, Soft Matter Phys.*, 2001, **6402**, 021514.
13 S. Asakura and F. Oosawa, *J. Chem. Phys.*, 1954, **22**, 1255.
14 S. Asakura and F. Oosawa, *J. Polym. Sci.*, 1958, **33**, 183.
15 A. Vrij, *Pure Appl. Chem.*, 1976, **48**, 471.
16 D. Rudhardt, C. Bechinger and P. Leiderer, *Phys. Rev. Lett.*, 1998, **81**, 1330.
17 Y. N. Ohshima, *et al.*, *Phys. Rev. Lett.*, 1997, **78**, 3963.
18 S. M. Ilett, A. Orrock, W. C. K. Poon and P. N. Pusey, *Phys. Rev. E: Stat. Phys., Plasmas, Fluids, Relat. Interdiscip. Top.*, 1995, **51**, 1344.
19 E. J. Meijer and D. Frenkel, *Phys. Rev. Lett.*, 1991, **67**, 1110.
20 E. J. Meijer and D. Frenkel, *J. Chem. Phys.*, 1994, **100**, 6873.
21 A. P. Gast, C. K. Hall and W. B. Russel, *J. Colloid Interface Sci.*, 1983, **96**, 251.
22 H. N. W. Lekkerkerker, W. C. K. Poon, P. N. Pusey, A. Stroobants and P. B. Warren, *Europhys. Lett.*, 1992, **20**, 559.
23 F. L. Calderon, J. Bibette and J. Bais, *Europhys. Lett.*, 1993, **23**, 653.
24 A. Hanke, E. Eisenriegler and S. Dietrich, *Phys. Rev. E: Stat. Phys., Plasmas, Fluids, Relat. Interdiscip. Top.*, 1999, **59**, 6853.
25 S. Ramakrishnan, M. Fuchs, K. S. Schweizer and C. F. Zukoski, *J. Chem. Phys.*, 2002, **116**, 2201.
26 S. Ramakrishnan, M. Fuchs, K. S. Schweizer and C. F. Zukoski, *Langmuir*, 2002, **18**, 1082.

27 P. B. Warren, S. M. Ilett and W. C. K. Poon, *Phys. Rev. E: Stat. Phys., Plasmas, Fluids, Relat. Interdiscip. Top.*, 1995, **52**, 5205.
28 R. Dickman and A. Yethiraj, *J. Chem. Phys.*, 1994, **100**, 4683.
29 A. Hanke, E. Eisenriegler and S. Dietrich, *Phys. Rev. E: Stat. Phys., Plasmas, Fluids, Relat. Interdiscip. Top.*, 1999, **59**, 6853.
30 F. Schelesenger, A. Hanke, R. Klimpel and S. Dietrich, *Phys. Rev. E: Stat., Nonlinear, Soft Matter Phys.*, 2001, **63**, 041803.
31 A. A. Louis, P. G. Bolhuis, E. J. Meijer and J. P. Hansen, *J. Chem. Phys.*, 2002, **117**, 1893.
32 R. Verma, J. Crocker, T. Lubensky and A. Yodh, *Phys. Rev. Lett.*, 1998, **81**(18), 4004.
33 J. Joanny, L. Leibler and P.-G. de Gennes, *J. Polym. Sci.*, 1979, **17**, 1073.
34 X.-Z. Cao, H. Merlitz, C.-X. Wu and J.-U. Sommer, *Phys. Rev. E: Stat., Nonlinear, Soft Matter Phys.*, 2011, **84**, 041802.
35 A. L. Frischknecht and A. Yethiraj, *J. Chem. Phys.*, 2011, **134**, 174901.
36 A. Bymaster, S. Jain and W. G. Chapman, *J. Chem. Phys.*, 2008, **128**, 164910.
37 J. B. Hooper, K. S. Schweizer, T. G. Desai, R. Koshy and P. Keblinski, *J. Chem. Phys.*, 2004, **121**, 6986.
38 H. N. W. Lekkerkerker and R. Tuinier, *Colloids and the Depletion Interaction*, Springer, Dordrecht Heidelberg Lonon New York, 2011.
39 N. Patel and S. A. Egorov, *J. Chem. Phys.*, 2004, **121**, 4987.
40 S. A. Egorov, *Phys. Rev. E: Stat., Nonlinear, Soft Matter Phys.*, 2004, **70**, 031402.
41 S. A. Egorov, *Phys. Rev. E: Stat., Nonlinear, Soft Matter Phys.*, 2005, **72**, 010401.
42 N. Patel and S. A. Egorov, *J. Am. Chem. Soc.*, 2005, **127**, 14124.
43 N. Patel and S. A. Egorov, *J. Chem. Phys.*, 2005, **123**, 144916.
44 S. A. Egorov, *J. Chem. Phys.*, 2007, **127**, 184903.
45 N. L. McFarlane, N. J. Wagner, E. W. Kaler and M. L. Lynch, *Langmuir*, 2010, **26**(17), 13823.
46 K. Kremer, *J. Chem. Phys.*, 1990, **92**, 5057.
47 M. Murat and G. Grest, *Phys. Rev. Lett.*, 1989, **63**, 1074.
48 M. Somasi, B. Khomami, N. J. Woo, J. S. Hur and E. S. G. Shaqfeh, *J. Non-Newtonian Fluid Mech.*, 2002, **108**, 227.
49 S. Plimpton, *J. Comput. Phys.*, 1995, **117**, 1.
50 J. C. Crocker, J. A. Matteo and A. D. Dinsmore, *Phys. Rev. Lett.*, 1999, **82**(21), 4352.
51 R. Roth, R. Evans and S. Dietrich, *Phys. Rev. E: Stat. Phys., Plasmas, Fluids, Relat. Interdiscip. Top.*, 2000, **62**(4), 5360.
52 M. Doxastakis, Y.-L. Chen, O. Guzman and J. J. de Pablo, *J. Chem. Phys.*, 2004, **120**(19), 9335.
53 P.-G. de Gennes, *Scaling Concepts in Polymer Physics*, Cornell University Press, Ithaca and London, 1979.
54 S. Yang, D. Yan, H. Tan and A.-C. Shi, *Phys. Rev. E: Stat., Nonlinear, Soft Matter Phys.*, 2006, **74**, 041808.
55 A. A. Louis, R. Finken and J. P. Hansen, *Phys. Rev. E: Stat. Phys., Plasmas, Fluids, Relat. Interdiscip. Top.*, 2000, **61**, R1028.
56 R. Tuinier, J. K. G. Dhnot and C. G. D. Kruif, *Langmuir*, 2000, **16**(4), 1497.
57 J. L. Doublier, C. Garnier, D. Renard and C. Sanchez, *Curr. Opin. Colloid Interface Sci.*, 2000, **5**, 202.
58 R. P. Sear, *Phys. Rev. E: Stat. Phys., Plasmas, Fluids, Relat. Interdiscip. Top.*, 1997, **56**, 4463.

